Erbium Doped SiO_2 Layers Formed on the Surface of Silicon by Spark Processing

John V. St. John and Jeffery L. Coffer*

Department of Chemistry, Texas Christian University, Fort Worth, Texas 76129

Young G. Rho, Patrick Diehl, and Russell F. Pinizzotto*

Department of Materials Science, University of North Texas, Denton, Texas 76203

Thomas D. Culp and Kevin L. Bray*

Department of Chemical Engineering, University of Wisconsin, Madison, Wisconsin 53706

Received July 8, 1997. Revised Manuscript Received August 27, 1997[⊗]

We present structural and spectroscopic analyses of luminescent erbium-doped porous SiO_2 layers on silicon formed using a spark processing technique. Scanning electron microscopy reveals a surface of irregular holes covered by a SiO_2 layer. Concomitant energy-dispersive X-ray mapping experiments show that the erbium concentration in the porous layer can be controlled by varying the molarity of the erbium solution deposited on the substrate prior to spark processing. Both visible and near-infrared photoluminescence spectroscopy, under conditions of varying temperature and excitation power, have been used to study the nature of the erbium centers formed in the porous layer. Self-quenching of Er^{3+} photoluminescence at 1.54 μm occurs at the highest concentrations of erbium employed.

Introduction

There has been extensive effort in the past few years to incorporate rare-earth ions into semiconductor substrates, primarily for optoelectronic purposes.[1,2] The rare-earth ion erbium is of particular interest because of the $(^4I_{13/2})\rightarrow(^4I_{15/2})$ transition and the resulting luminescence band at 1.54 μm, which lies at an absorption minimum for silica-based optical fibers and glasses. The most widespread method for doping semiconductors with Er^{3+} is ion implantation.[1−8] However, more facile methods such as diffusion,[9] potential-assisted diffusion,[10] and spark processing[11] have been under recent investigation.

Studies have shown that the high-frequency arc from a tesla coil can ablate the surface of crystalline silicon, leaving behind a porous layer capped with SiO_2.[12−16] If a rare-earth salt is deposited on the silicon surface and then spark processed, the resulting Si porous layer and SiO_2 cap are doped with "clusters" of rare-earth ions coordinated to oxygen.[11] This highly energetic process leaves behind a surface with irregular holes and "cauliflower" shaped clusters of SiO_2 and can be adapted to introduce any rare-earth ion into a silicon surface.

In this paper we present a study of erbium-doped silicon produced by the spark processing of erbium nitrate deposited on the surface of single-crystal silicon. It is shown that the relative amount of Er^{3+} in the spark-processed layers is a function of the initial erbium nitrate concentration deposited on the surface before spark processing. Visible and near-IR photoluminescence (PL) measurements demonstrate that the concentration of Er^{3+} is proportional to the intensity of the visible fluorescence transitions; self-quenching of the near-IR fluorescence peak at 1.54 μm due to erbium clustering occurs at higher Er^{3+} concentrations. PL intensity measurements of the 1.54 μm Er^{3+} transition as a function of excitation power and temperature show a sublinear increase in intensity with increasing power.

Experimental Section

Square pieces (15 mm × 15 mm) of *p*-type, ⟨100⟩ , boron-doped CZ Si (6−8 Ω cm) were used as substrates in these experiments. Metallic contact was made to the back of the wafers using Ni wire and Ag epoxy. Thin layers of $Er(NO_3)_3$·

* To whom correspondence should be addressed.

[⊗] Abstract published in *Advance ACS Abstracts,* November 1, 1997.

(1) Ennen, H.; Schneider, J.; Pomrenke, G.; Axmann, A. *Appl. Phys. Lett.* **1983**, *90*, 943.
(2) Ennen, H.; Pomrenke, G.; Axmann, A.; Eisele, K,; Haydl, W.; Schneider, J. *Appl. Phys. Lett.* **1985**, *46*, 381.
(3) Benton, J. L.; Michel, J.; Kimerling, L. C.; Jacobson, D. C.; Xie, Y.-H.; Eaglesham, D. J.; Fitzgerald, E. A.; Poate, J. M. *J. Appl. Phys.* **1991**, *70*, 2667.
(4) Adler, D. L.; Jacobsen, D. C.; Eaglesham, D. J.; Marcus, M. A.; Benton, J. L.; Poate, J. M.; Citrin, P. H. *Appl. Phys. Lett.* **1992**, *61*, 2181.
(5) Coffa, S.; Franzò, G.; Priolo, F.; Polman, A.; Serna, R. *Phys. Rev. B* **1994**, *49*, 313.
(6) Lombardo, S.; Campisano, S. U.; van den Hoven, G. N.; Polman, A. *Nucl. Instrum. Methods B* **1995**, *96*, 378.
(7) Namavar, F.; Lu, F.; Perry, C. H.; Cremins, A.; Kalkhoran, N. M.; Soref, R. A. *J. Appl. Phys.* **1995**, *77*, 4813.
(8) Hömmerich, U.; Namavar, F.; Cremins, A.; Bray, K. *Appl. Phys. Lett.* **1996**, *68*, 1951.
(9) Lin, J.; Zhang, L. Z.; Huang, Y. M.; Zhang, B. R.; Qin, G. G. *Appl. Phys. Lett.* **1994**, *64*, 3282.
(10) Kimura, T.; Yokoi, A.; Horiguchi, H.; Saito, R.; Ikoma, T.; Sato, A. *Appl. Phys. Lett.* **1994**, *65*, 983.
(11) St. John, J. V.; Coffer, J. L.; Rho, Y. G.; Pinizzotto, R. F. *Appl. Phys. Lett.* **1996**, *68*, 3416.
(12) Hummel, R. E.; Chang, S.-S. *Appl. Phys. Lett.* **1992**, *61*, 1965.
(13) Hummel, R. E.; Morrone, A.; Ludwig, M. H.; Chang, S.−S. *Appl. Phys. Lett.* **1993**, *63*, 2771.
(14) Hummel, R. E.; Ludwig, M. H. *J. Lumin.* **1996**, *68*, 69.
(15) Priolo, F.; Coffa, S.; Franzò, G.; Spinella, C.; Carnera, A.; Bellani, V. *J. Appl. Phys.* **1993**, *74*, 4936.
(16) Polman, A,; van den Hoven, G. N.; Cluster, J. S.; Shin, J. H.; Serna, R.; Alkemade, P. F. A. *J. Appl. Phys.* **1995**, *77*, 1256.

S0897-4756(97)00477-8 CCC: $14.00

$5H_2O$ were deposited on the surfaces of silicon wafers by allowing a dilute solution of the salt to evaporate. The samples were coated by depositing 10 or 25 μL of a solution via syringe onto the wafer surface. The concentrations ranged from 0.01 to 0.5 M $Er(NO_3)_3 \cdot 5H_2O$ in water. Upon evaporation of the solvent, circular layers of erbium salt crystals approximately 3 mm in diameter remain on the wafer surface.

Spark processing was performed by connecting the sample to the cathode of an Electro Technics Products tesla coil which produced a high-frequency (15 kHz), high-voltage (10 kV), low-current (several mA) spark. An untreated silicon wafer was used as the anode. The arc from the coil migrates over the silicon substrate, and the size of the spark processed region is a function of the spark gap. The gap was adjusted so that the entire layer of rare earth crystals was processed by the arc. Samples were processed in air for 60 min. After processing, samples were washed with deionized H_2O, ethanol, and acetone and then dried under a stream of dry nitrogen. Some samples were further processed using rapid thermal oxidation (RTO) in air with a Modular Process Technology Corp. RTP 610. The RTO samples were heated to 1100 °C for 4 min using a 100 °C/s ramp rate.

Low-resolution (±4 nm) near-IR photoluminescence (PL) spectra were obtained using an Applied Detector Corp. liquid N_2 cooled Ge detector in conjunction with a Stanford Research Systems chopper/lock-in amplifier and an Acton Research Corp. 0.25 m monochromator. Excitation was provided by a coherent Ar^+ laser. High-resolution (±0.1−0.5 nm) near-IR and visible PL spectra were obtained by excitation with the 488 nm line of a coherent Ar^+ laser. The resulting fluorescence was focused on the entrance slit of a Spex 1 m monochromator with a photomultiplier tube used to detect visible PL, and a liquid N_2 cooled Ge detector used for near-IR PL measurements. Cooling for all PL measurements was achieved by mounting the sample in a Janis closed cycle helium cryostat.

Scanning electron microscopy (SEM) was performed using a JEOL T 300 operating at 20 kV. Energy-dispersive X-ray mapping was performed using a Tracor-Northern TN5500 system. The spark processed region was analyzed for Si and Er atoms, and separate Si and Er concentration maps of the same area were obtained. MCID software from Imaging Research Inc. was used to quantify the X-ray concentration data in the spark processed regions. Measured Er-to-Si ratios were used to determine the relative density of Er^{3+} in the spark-processed regions for varying initial Er^{3+} concentrations.

Results and Discussion

The spark-processing technique causes the high-energy ablation of the silicon surface, which is oxidized to form a porous SiO_2 layer. When present on the surface, rare-earth centers can become trapped in the local condensing SiO_2 during spark processing.[11] Control samples (with no rare-earth elements present on the surface) subjected to spark processing show no visible PL due to spark processed silicon nanoclusters. Unlike previous work,[12−14] the apparatus used in our experiments does not produce the small (<2 nm) Si nanoparticles required for efficient visible light emission. A scanning electron micrograph of an Er-doped wafer surface after processing is shown in Figure 1. The surface is composed of irregular holes surrounded by nonuniform clusters of SiO_2. The depth of the spark-processed layer is dependent on processing time. SEM cross-sectional measurements show that the layer extends 10−15 μm into the crystalline substrate after 60 min of processing.

Energy-dispersive X-ray mapping in the SEM was used to determine the effect of initial Er^{3+} salt concentration on the resulting relative ratios of erbium to Si in the porous layers. X-ray maps of a spark-processed erbium/silicon wafer with an initial Er^{3+} concentration

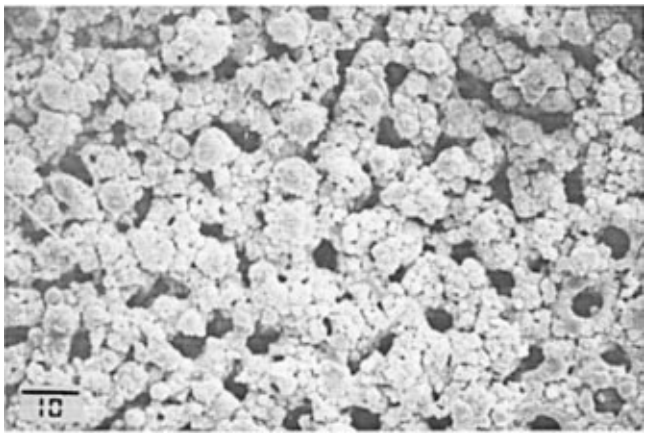

Figure 1. Scanning electron micrograph of an Er-doped ⟨100⟩ Si substrate after 60 min of spark processing. The scale bar is 10 μm.

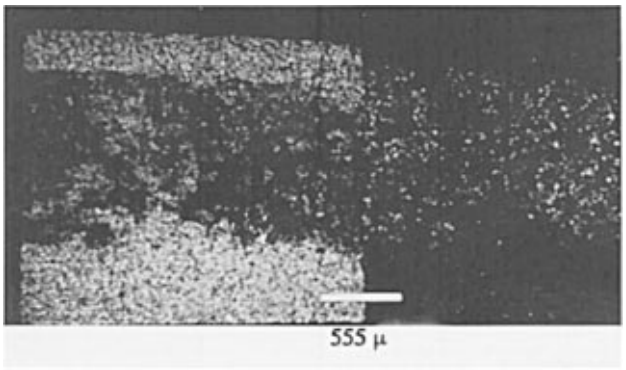

Figure 2. Energy-dispersive X-ray maps of a ⟨100⟩ Si substrate illustrating the effects of 60 min of spark processing. The substrate was coated with 0.1 M $Er(NO_3)_3 \cdot 5H_2O$. The left side of the figure shows the Si density in the spark processed layer, while the right side shows the Er density in the same region. Note that the Er atoms are essentially confined within the porous layer.

of 0.1 M and processed for 60 min are shown in Figure 2. The left side of the figure shows a map of the silicon concentration inside the spark processed region. Note that the spark processed region has a much lower Si density than the surrounding crystalline silicon substrate due to the ablation of the substrate and the presence of SiO_2. The right side of the figure shows the erbium density in the spark-processed region. A plot of the Er/Si ratio vs initial Er^{3+} solution concentration for samples ranging from 0.1 to 0.4 M $Er(NO_3)_3 \cdot 5H_2O$ in H_2O is shown in Figure 3. A clear increase in Er-to-Si ratio with increasing Er^{3+} concentration is observed, indicating that the density of Er atoms in the SiO_2 layer can be controlled by varying the initial $Er(NO_3)_3 \cdot 5H_2O$ concentration deposited on the Si substrate prior to spark processing.

The 1.54 μm luminescence of the spark processed Er^{3+} on Si at low resolution shows changes in intensity with increasing concentration of the initial $Er(NO_3)_3 \cdot 5H_2O$ solution. Figure 4 shows the room-temperature near-IR PL spectra of five samples treated with 10 μL of 0.1−0.5 M $Er(NO_3)_3 \cdot 5H_2O$ before spark processing. The PL intensity at 1.54 μm is observed to increase with increasing Er^{3+} concentration up to 0.4 M. Increasing the $Er(NO_3)_3 \cdot 5H_2O$ concentration to 0.5 M results in a dimunition of the near-IR PL. The decrease in relative intensity of spark-processed samples treated with more

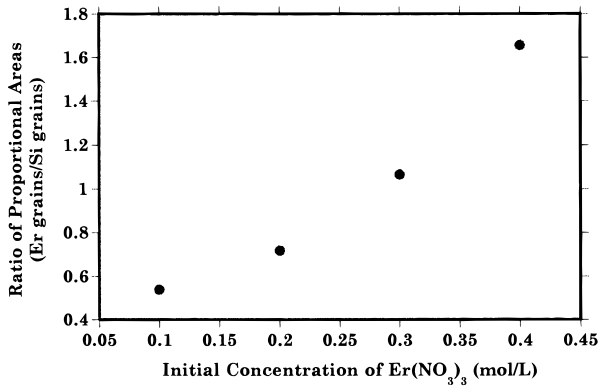

Figure 3. Plot of Er/Si pixel density vs concentration (M) for ⟨100⟩ Si samples that have been coated with 0.1−0.4 M $Er(NO_3)_3 \cdot 5H_2O$ and spark processed in air for 60 min.

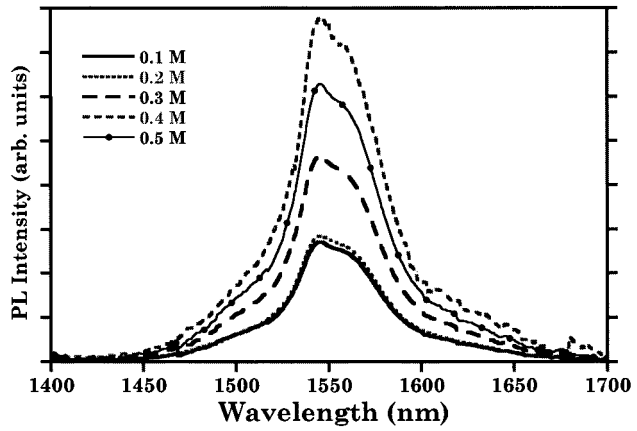

Figure 4. Low-resolution near-IR PL spectra at 1.54 μm for samples that have been coated with of 0.1−0.5 M $Er(NO_3)_3 \cdot 5H_2O$ and then exposed to 60 min of spark processing in air. Excitation was provided by the 488 nm line of an argon-ion laser.

concentrated erbium solutions is believed to be caused by self-quenching due to erbium aggregation in the spark-processed layer. These Er precipitates, which have been shown to form during ion implantation at higher doses, act as sites for nonradiative recombination.[15] It should also be pointed out that the minor differences in PL intensity between low initial Er^{3+} concentrations (e.g., between 0.1 and 0.2 M) and larger differences in PL between samples at higher initial Er^{3+} concentrations is also consistent with the differences in the observed Er/Si ratios illustrated in the X-ray map (Figure 3). In explaining these observations, there are several possibilities to consider: (1) Increasing the concentration to 0.2 M results in the additional Er occupying spatial positions (either in terms of depth or lateral dimension) not occupied at 0.1 M, i.e., some of the Er is outside of the laser beam (2) Er enters the substrate in different ways, e.g., a balance exists between so-called optically active and inactive Er. Clustering is one way to create inactive Er. Other possibilities might involve interstitial versus substutional sites, although this is certainly more ambiguous in a porous layer. (3) The scenario that some Er is blasted from the surface in the 0.2 M case is a possibility, although one might anticipate that this would result in erratic flucuations in near-IR PL intensity as a function of Er^{3+} concentration, which is not the case in our experiments (repeated five times).

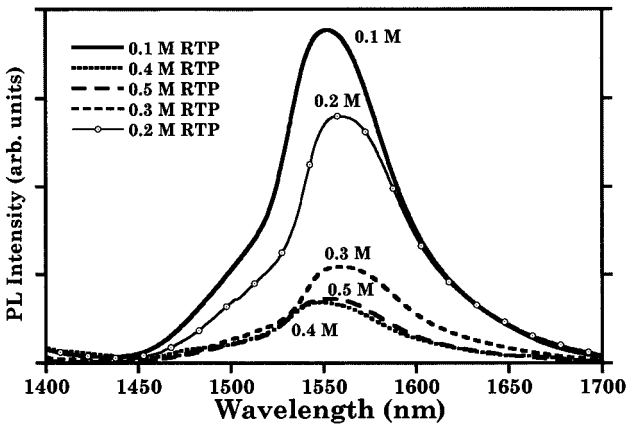

Figure 5. Low-resolution near-IR PL spectra at 1.54 μm for samples that have been coated with 0.1−0.5 M $Er(NO_3)_3 \cdot 5H_2O$, exposed to 60 min of spark processing in air and then rapid thermally processed for 4 min at 1100 °C. Excitation was provided by the 488 nm line of an argon-ion laser.

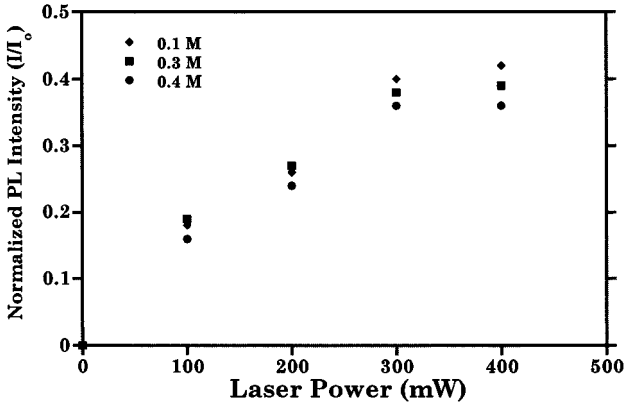

Figure 6. Normalized intensity of the 1.54 μm Er transition vs laser power at 488 nm for samples which have been coated with 0.1−0.5 M $Er(NO_3)_3 \cdot 5H_2O$ and then exposed to 60 min of spark processing in air.

The 1.54 μm low-resolution PL of spark-processed samples which have been rapid thermally annealed (RTA) in air to 1100 °C for 4 min demonstrates different behavior than samples that have not been heated in this manner. Figure 5 shows low-resolution near IR PL spectra for samples with 10 μL of $Er(NO_3)_3 \cdot 5H_2O$ at concentrations from 0.1 to 0.5 M with a 4 min 1100 °C RTP in air. Rapid thermally annealed silicon samples with lower initial erbium concentrations (≤0.2 M) have near-IR PL intensities up to 3 times stronger than samples that have not been annealed. Annealed samples prepared with initial Er^{3+} concentrations above 0.2 M show lower relative PL intensities than annealed samples prepared with 0.1 or 0.2 M $Er(NO_3)_3 \cdot 5H_2O$. Unannealed samples always show weaker luminescence than annealed samples for all Er^{3+} concentrations. The stronger PL intensity of samples that are rapid thermally processed relative to nonannealed samples is attributed to optical activation of erbium centers forming a coordination shell of oxygen atoms which inhibit nonradiative pathways for Er^{3+} ions.[4,15] The relatively lower PL intensities of the samples with higher concentrations of Er are again attributed to the presence of erbium precipitates which may form more readily during the high-temperature anneal.

Figure 6 shows the dependence of the room-temperature PL intensity at 1.54 μm on laser power for samples

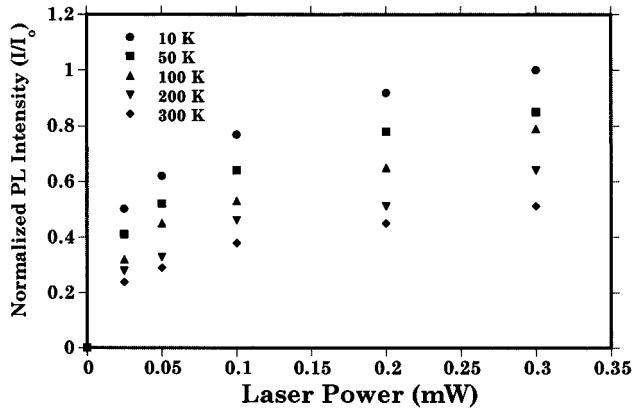

Figure 7. Normalized intensity (at 10 K, 300 W) of the 1.54 μm Er luminescence peak at temperatures of 10, 100, 200, and 300 K vs laser power at 488 nm for a sample coated with 0.3 M $Er(NO_3)_3 \cdot 5H_2O$ and then exposed to 60 min of spark processing in air.

which were treated with 0.1, 0.3, and 0.5 M $Er(NO_3)_3 \cdot 5H_2O$ and then spark processed for 60 min. The PL intensity of Er^{3+} at 1.54 μm for all concentrations is proportional to the square root of the pump laser power. This sublinear PL power dependency has been reported for Er^{3+} doped in several systems.[5,8,10,16] Figure 7 shows the PL intensity at 1.54 μm as a function of pump power at 488 nm and temperatures of 10, 100, 200, and 300 K for a sample treated with 10 μL of 0.3 M $Er(NO_3)_3 \cdot 5H_2O$ and then spark processed. The PL power dependency vs temperature also shows a sublinear power dependence at each temperature. Two mechanisms have been proposed to explain the sublinear power dependency for Er^{3+} in crystalline semiconductors: (1) saturation of optically active Er^{3+} centers with exciting light[17] and (2) nonradiative Auger quenching can occur at excitation saturation levels as energy from electron/hole recombination is transferred to electrons and then to the surrounding silicon matrix as heat.[18] In this case, as Er is embedded in a SiO_2 matrix, the number of free carriers will be too low for this likely to be an important process.

Figure 8 shows the high-resolution visible luminescence spectrum for the $(^4S_{13/2}) \rightarrow (^4I_{15/2})$ transition near 560 nm (at 14 K) for samples that have been spark processed with 0.01, 0.1, and 0.5 M $Er(NO_3)_3 \cdot 5H_2O$ using a 3.0 mm diameter mica mask to form a well-defined circular spark processed region on the Si substrate. These samples were processed using a 4 min rapid thermal anneal to 1100 °C after spark processing. The visible Er PL corresponding to the $(^4S_{13/2}) \rightarrow (^4I_{15/2})$ transition at 560 nm and the $(^4F_{9/2}) \rightarrow (^4I_{15/2})$ transition at 670 nm (not shown) show increases in intensity with increasing initial $Er(NO_3)_3 \cdot 5H_2O$ concentration. The large number of sharp peaks at each manifold in the high-resolution spectra indicate that several different Er^{3+} centers are present. The $^4I_{15/2}$ manifold can be split into a maximum of eight Stark levels for each Er^{3+} ion environment, indicating that more than one different site symmetry is present for erbium in spark-processed silicon.

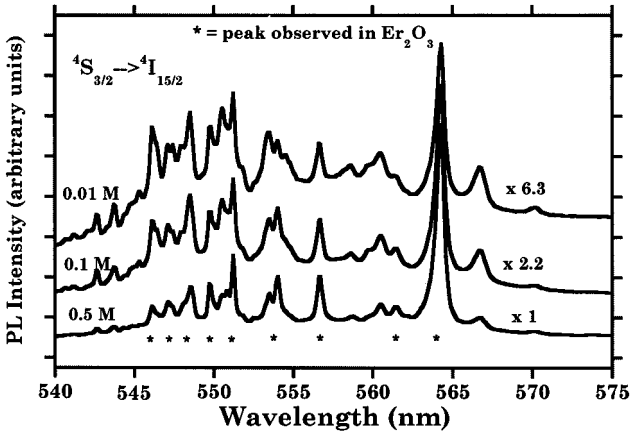

Figure 8. High-resolution (±0.1 nm) PL spectra of the visible $(^4S_{13/2}) \rightarrow (^4I_{15/2})$ transitions at 14 K for samples that have been coated with 0.01, 0.1, and 0.5 M $Er(NO_3)_3 \cdot 5H_2O$ and then exposed to 60 min of spark processing in air through a mica mask.

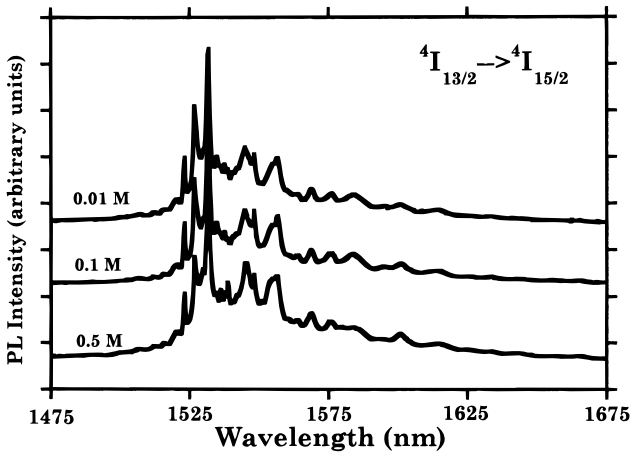

Figure 9. High-resolution (±0.4 nm) near-IR PL spectra of the $(^4I_{13/2}) \rightarrow (^4I_{15/2})$ transition at 14 K for samples that have been coated with 0.01, 0.1, and 0.5 M $Er(NO_3)_3 \cdot 5H_2O$ and then exposed to 60 min of spark processing in air through a mica mask.

High-resolution near-infrared PL in the 1540 nm region for spark processed Er on silicon has also been measured at 14 K. In Figure 9, high-resolution PL spectra are shown for samples that have been spark processed with 25 μL of 0.01, 0.1, and 0.5 M $Er(NO_3)_3 \cdot 5H_2O$. In these samples, the area of the erbium salt processed by the spark was also controlled with a mica mask, and the samples were then rapid thermally processed at 1100 °C. The intensity of the $(^4I_{13/2}) \rightarrow (^4I_{15/2})$ transition at 1.5316 μm for these samples does not clearly increase with increasing Er^{3+} concentration, because of greater variations in intensity at different points within the spark processed region (indicative of nonuniform clustering of Er centers within the mica-induced "pellet"). It is important to note that as in the case of the high-resolution visible PL spectra, the multiple peaks (>20) in the near-infrared region at 14 K are consistent with the existence of Er^{3+} ions incorporated in several site symmetries within the porous host matrix.

We have also measured the decay lifetimes of these peaks at 14 K. All samples exhibit an identical decay curve which can be fit using a single exponential with $\tau \sim 0.27 \pm 0.02$ ms. However, this decay time is very close to the detector response time (~0.20 ms). Thus,

(17) Coffa, S.; Priolo, F.; Franzò, G.; Bellani, V.; Carnera, A.; Spinella, C. *Phys. Rev. B* **1993**, *48*, 11782−11788.
(18) Benton, J. L.; Eaglesham, D. J.; Almonte, M.; Citrin, P. H.; Marcus, M. A.; Adler, D. L.; Jacobsen, D. C.; Poate, J. M. *Mater. Res. Soc. Symp.* **1990**, *301*, 119.

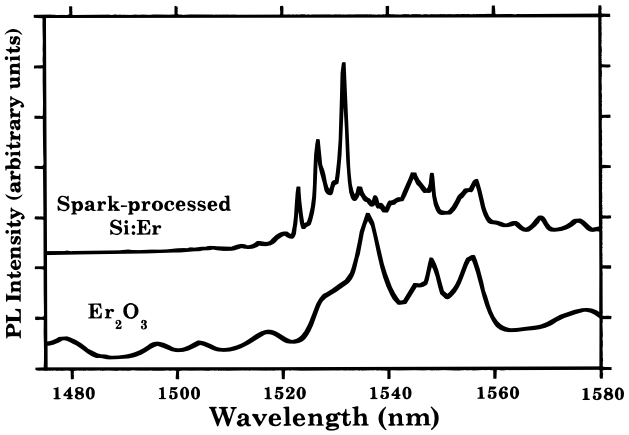

Figure 10. Comparison of the high-resolution near-IR PL spectra of the $(^4I_{13/2})\rightarrow(^4I_{15/2})$ transition at low temperature between Er_2O_3 (resolution ±0.48 nm) and a typical spark processed Er^{3+} doped Si sample (resolution ±0.4 nm).

the observed curve is a convolution of the detector response and the true decay. The true lifetime will be less than 0.27 ms, possibly in the 0.1 to 0.2 ms range. It is not possible to estimate the true lifetime differences between samples, and the only conclusion that can be drawn is that all three samples exhibit a fast decay of less than 0.27 ms. The other emission peaks (1.5229, 1.5266, 1.5448, 1.5565, and 1.5837 μm) also exhibit the same fast decay ($\lesssim$0.27 ms) as that of the l.5316 μm peak. In any case, such fast decay is consistent with energy transfer between Er centers, i.e., clustering. Typical low-temperature lifetimes for most Er-doped semiconductor hosts are on the order of a millisecond; for example, a lifetime of 0.9 ms has been observed in GaAs:Er[19] and 1.2 ms in GaP:Er.[20]

Finally, it should be pointed out that when one compares the high-resolution PL spectra (both visible and near-infrared) of spark-processed erbium-doped porous SiO_2 layers on silicon with those for crystalline erbium oxide (Er_2O_3), many peaks match those observed in Er_2O_3, although the relative intensities vary (Figure 10). However, many peaks observed in Er_2O_3 are not observed in the spark-processed erbium-doped Si and vice versa. The line widths in Er_2O_3 powder tend to be larger, although this could be related to the strong H_2O adsorption of the powder. Thus, although there are many similarities between the Er centers in the oxide layer and Er_2O_3, it is unlikely that the spark-processed Er forms a distinct, pure Er_2O_3 phase. It should be noted, however, that from a close scrutiny of Figure 8 there seems to be a decrease in the relative intensity of peaks not occurring in Er_2O_3 relative to those that do occur in Er_2O_3 as the Er concentration increases. This would support the argument that the relative amount of Er_2O_3 clusters/precipitates increases as the concentration of Er increases. Again, in Figure 8, one can see roughly six features not present in Er_2O_3. This suggests that in these spark-processed layers there exists a combination of a well-defined Er site and a Er_2O_3-like phase, with the latter growing with increasing Er.

(19) Culp, T. D.; Hömmerich, U.; Redwig, J. W.; Kuech, T. F.; Bray, K. *J. Appl. Phys.* **1997**, *82*, 368.
(20) Culp, T. D.; Wang, X. Z.; Kuech, T. F.; Wessels, B. W.; Bray, K. *Mater. Res. Soc. Symp. Proc.* **1996**, *422*, 279.

Conclusions

Spark processing of erbium salts on silicon surfaces produces erbium coordinated to oxygen in a layer of SiO_2 which shows luminescence from the near-IR $(^4I_{13/2})\rightarrow(^4I_{15/2})$ transition at 1540 nm as well as the $(^4S_{13/2})\rightarrow(^4I_{15/2})$ and $(^4F_{9/2})\rightarrow(^4I_{15/2})$ visible transitions at 560 and 670 nm, respectively. The surfaces after spark processing are characterized by rough porous clusters of SiO_2. The concentration of erbium within the spark processed region is dependent on the initial concentration of erbium salt on the surface before spark processing and can be varied by simply increasing or decreasing the molarity of the $Er(NO_3)_3{\cdot}5H_2O$. At higher erbium concentrations, self-quenching occurs, probably due to erbium clustering or precipitates. This clustering decreases the luminescence intensity. Samples that have been spark processed and then exposed to a rapid thermal annealing treatment in air exhibit stronger luminescence than samples without RTA; however, self-quenching occurs at lower concentrations in these materials than samples that have not been thermally processed. Patterns of erbium in spark processed silicon can be formed using mica masks; however this causes nonuniform distribution of the erbium centers.

It is believed that further work using this system will yield improved Er-doped SiO_2 suitable for waveguides or similar components on silicon surfaces.

Acknowledgment. Financial support by the Texas Advanced Technology Program and the Robert A. Welch Foundation to J.L.C. are gratefully acknowledged. K.L.B. gratefully acknowledges support from the National Science Foundation under Grant DMR 95-10139 as well as the NSF Division of International Programs. T.D.C. acknowledges fellowship support from the University of Wisconsin.

CM970477I